17th World Conference on Earthquake Engineering, 17WCEE
Sendai, Japan - September 13th to 18th 2020

EVALUATION OF LONG-PERIOD GROUND MOTIONS IN THE ASO CALDERA DURING THE 2016 KUMAMOTO EARTHQUAKE

T. Kidoh[(1)], M. Nagano[(2)]

[(1)] *Shimizu Corporation (Former affiliation: Graduate Student, Tokyo University of Science), 7114034@alumni.tus.ac.jp*
[(2)] *Professor, Tokyo University of Science, nagano-m@rs.noda.tus.ac.jp*

Abstract

During the main event of the 2016 Kumamoto earthquake (M_W7.0), Japan, surface ruptures were confirmed in a wide region and were accompanied by a broad area of crustal deformation. In the vicinity of the surface ruptures, seismic intensities of scale 7 on the Japan Meteorological Agency (JMA) intensity scale and large-amplitude pulse-type ground motions were observed. In Mashiki Town, large-amplitude pulse-type ground motions with periods of 1 sec were observed in a direction parallel to the fault. These pulse-type ground motions caused severe damage to wooden houses and resulted in a zone of damage with a width of approximately 1 km in the central part of Mashiki Town. Moreover, at Nishihara Village and at the K-NET Ichinomiya (KMM004) seismograph station, long-period pulses with a dominant period of approximately 3 sec were observed, which might cause damage to long-period structures including super-high-rise buildings and seismically isolated buildings. For a seismically isolated building in Aso City (approximately 3.5 km away from the KMM004 station), the maximum relative displacement of isolation detected from orbiter was smaller than expected from the records at KMM004. This implies that the amplitudes of long-period ground motions vary spatially depending on distances from to the seismic faults and on different site amplification levels.

In this study, we constructed a characterized fault model consisting of a background region, SMGA (Strong Motion Generation Area) and LMGA (Long-period Motion Generation Area) and performed theoretical simulations of strong ground motions and permanent displacements around the seismic fault. From the comparisons between the distributions of building damage areas in the Mashiki Town and the theoretical simulated ground motions, we determined that the upper boundary of SMGA is approximately 2 km deep and that the LMGA is shallower. Using the characterized fault model, the strong motion records around the seismic faults were reproduced well. The generation of large-amplitude pulses in Mashiki Town and Nishihara Village is attributed to multiple fault ruptures, upward rupture directivity effects, and slip ruptures near the ground surface (LMGA). By setting the southeast-dipping segment in Aso Caldera at the northeastern part of the Futagawa fault zone and the two SMGAs in it, we were able to reproduce the subsidence trends in Aso Caldera and the long-period ground motions at KMM004. Other strong motion records obtained in Aso Caldera were well reproduced but the contribution of the segment in Aso Caldera to the simulated waveforms was relatively small. The long-period ground motions in Aso Caldera were not due to surface ruptures (LMGA), but instead were due to the directivity effects of the deep SMGAs and site amplification. The ground motions at a seismically isolated building in Aso City were simulated using the characterized fault model. The velocity structure model in Shigefuji *et al.* (2019), which is located at the site of the seismically isolated building, overestimates the strong ground motions and isolation responses compared with orbital plots. By assuming smaller S-wave velocities in the deep parts of the subsurface structure, ground motion components with periods of 3 to 4 sec decreased and resulted in isolation deformations that were consistent with the seismogram.

Keywords: 2016 Kumamoto earthquake, Surface rupture, Pulse-like ground motion, Long-period ground motion

1. Introduction

During the main event of the 2016 Kumamoto Earthquake (M_W7.0) that occurred in the Kumamoto region around Kumamoto Prefecture, Japan, surface ruptures were confirmed over a wide region [1] and were accompanied by a wide range of permanent displacements. In the vicinity of the seismic faults, seismic intensities of 7 on the JMA intensity scale at Mashiki Town and Nishiahra Village. In Mashiki Town (near the surface ruptures), large-amplitude pulse-type ground motions with periods of approximately 1 sec were observed at 2 sites, namely KMMH16 (KiK-net Mashiki) and 93051 (Mashiki Town Miyazono) and structural damage to old wooden houses was locally concentrated in the central part of Mashiki Town [2]. At site 93048 (Nishihara Village Komori), long-period large-amplitude pulse-type ground motions with periods of approximately 3 sec were observed. The peak ground velocity (PGV) of these strong motions exceeded 250 cm/s. These long-period pulses can cause serious damage to long-period structures such as super-high-rise buildings and isolated buildings. At KMM004 (K-NET Ichinomiya), long-period ground motions with ${}_pS_V$ values (h = 5%) of approximately 400 cm/s with periods of approximately 3 sec were observed and the Aso Shrine tower gate and worship, located approximately 1.8 km from the KMM004 site, collapsed. Also, in a seismically isolated hospital building in Aso City, located approximately 3.6 km from the KMM004 site, the relative displacement of the seismic layer as determined from the recorded orbiter showed smaller deformations at isolated devices than expected from the records at KMM004 [3]. This implies that the amplitudes of long-period ground motions spatially varied depending on the distances between the sites and the seismic faults and also depended on the differences in the site amplifications. Explaining the differences between these input ground motions using the theoretical ground motion calculated from the seismic fault model is important for predicting long-period ground motions to protect against future inland crustal earthquakes.

So far, many inversion analyses using strong motion waveforms and theoretical Green's functions have been conducted to estimate the heterogeneous slip distributions on the fault plane of the 2016 Kumamoto Earthquake [4, 5, 6, 7, 8], the Hinagu fault zone, and the Futagawa fault zone that extends into Aso Caldera, these inversions were commonly modeled using northwest dips. On the other hand, in a fault model based on geodetic data, a model with southeast dip was estimated for Aso Caldera [9]. In the seismic fault inversion analysis using strong motion waveforms performed by Yoshida *et al.* [7], the modeling of the seismic fault in Aso Caldera was examined for northwest and southeast dips and there was no significant difference in the slip distributions between the two models. However, it has been shown that the sensitivity of inversion analysis is poor for the fault segment in Aso Caldera and that comparisons with the crustal deformation distributions based on the models with northwest and southeast dips for the segment of the Futagawa fault in Aso Caldera zone and synthetic aperture radar (SAR) indicates that the southeast-dipping model is appropriate. In addition, slip partitioning has been pointed out in the Futagawa fault zone [10] and some models have indicated a normal slip fault (Idenokuchi fault) [8, 11, 12] that runs parallel to the Futagawa fault zone at a slightly lower dip angle. Many evaluations of the ground motions during the 2016 Kumamoto Earthquake were conducted using characterized fault model based on a heterogeneous fault model based on waveform inversion analysis and a fault model based on geodetic data. The surface ruptures near Mashiki Town where seismic JMA intensities of 7 were recorded, were confirmed to extend from the Hinagu fault zone and to extend to the central part of Mashiki Town. There are many fault models showing that the surface ruptures connect to the Hinagu fault [4, 5, 7] but there are also explanations from fault models of the fault plane passing through the surface ruptures (Kiyama fault) branch to the central part of Mashiki Town as the main fault and various outer fault planes are being studied [9, 13].

The authors have conducted ground motion evaluations near the seismic faults during the 2016 Kumamoto earthquake [14] and have studied the causes of large-amplitude velocity pulses in Mashiki Town and Nishihara Village, which recorded JMA seismic intensities of 7. On the other hand, the strong ground motion at KMM004 was not adequately simulated. In this study, we referred to the previous seismic fault models for the main event of the 2016 Kumamoto Earthquake and construct a characterized fault model that can adequately simulate the strong motion records around the seismic fault, including those at KMM004. Next, the generation mechanism of the long-period ground motions in Aso City was investigated. Finally, the differences between the observation records at KMM004 and the ground motion at a seismic isolated hospital in Aso City are discussed.

2. Outline of theoretical ground motion calculations

2.1 Calculation methods

Theoretical seismic ground motions are calculated using the thin layer method (TLM) [15, 16] and assume that a horizontal layered soil structure is present at the target observation site. This method is a theoretical ground motion calculation method that has been sufficiently validated by benchmark tests [17], including evaluations of permanent displacements. This method exhibits high calculation efficiency for the evaluation of Green's functions when there are many combinations of receiver and source points in the fault plane. The thin layer divisions of the horizontal layered soil structure were defined to be 1/8 or less of one S-wave wavelength and the range of the effective period was set to 0.5 sec or higher. The permanent displacements as the static solution were evaluated by using the solution at 1/81.92 Hz, which is the minimum frequency used in the calculations.

2.2 Target observation sites and setting of the horizontal layered soil structures

The target observation sites are the 6 K-NET observation sites, 4 KiK-net observation sites, 2 JMA observation sites, 8 local public entity sites, and 2 JR strong motion observation sites shown in Fig. 1. There are a total of 22 observation sites. Fig. 1 also shows the ground surface projection of the outer fault plane of the characterized fault model used in this study (black lines) and the surface rupture distribution from the AIST (National Institute of Advanced Industrial Science and Technology) (red lines) [18, 19]. Detailed parameters of the characterized fault model will be explained later. The horizontal layered soil structures were established by the following procedure.

1. The subsurface structure was extracted directly under each observation site from the J-SHIS V2 model [20].
2. For the K-NET and KiK-net observation sites, PS logging data published by the NIED were added to the shallow velocity structures.
3. The S-wave and P-wave velocities of the velocity structures were tuned using the solution mechanism for a the small earthquake (M_J5.1) that occurred in the Kumamoto region of Kumamoto Prefecture at approximately 18:10 on January 3, 2019 and are shown in Fig. 1.
4. Regarding the nonlinear characteristics when strong ground motions are applied to shallow ground, the step-by-step nonlinearity cannot be addressed by the TLM, so this nonlinearity is addressed by using

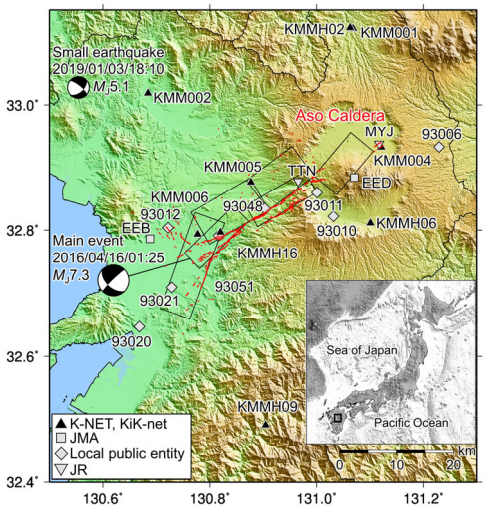

Fig. 1 – Target observation sites and surface ruptures distribution from AIST (2019). The beach ball show the mechanism of the small earthquake used for the tuning of velocity structures and main event of the 2016 Kumamoto Earthquake. The open squares show the outer fault plane of the characterized fault model in this study.

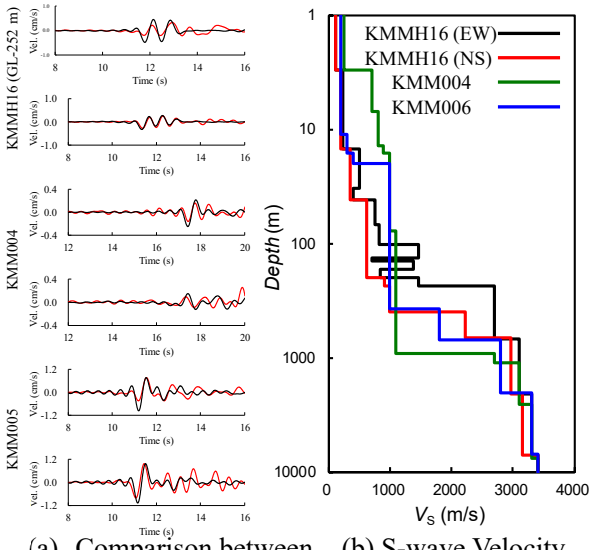

(a) Comparison between the observed waveforms (red lines) and synthetic waveforms (black lines)

(b) S-wave Velocity Structures at KMMH16, KMM004 and KMM006

Fig. 2 – Example of the tuning velocity structures.

equivalent S-wave velocities and equivalent damping coefficients. For the KiK-net observation sites, the equivalent parameters were determined by one-dimensional equivalent linear analysis using borehole-surface records. For other sites, the S-wave velocity of approximately V_S=1,000 m/s or less is easily multiplied by 0.75 and the damping constant was set to 5 % by referring to the tuned values at the KMMH16 site. The observation sites that considered the nonlinearity were the sites where the horizontal component of the PGV during the main event exceeded 30 cm/s.

However, since it was difficult to tune KMMH16 simultaneously for the NS and EW components, the soil structures were separately tuned for each component. In addition, the soil structures and nonlinearity parameters at site 93051 are the same as in the previous study [14]. As an example of tuning the velocity structures, Fig. 2 shows the simulation results of small earthquake records using the tuned S-wave velocity structures and the velocity structures at KMMH16, KMM004, and KMM006 (K-NET Kumamoto).

3. Characterized fault model and simulation of strong ground motion records

3.1 Outer and inner fault parameters of the characterized fault model

The characterized fault model is composed of three regions: strong motion generation area (SMGA), long-period motion generation area (LMGA), and background region. The outer fault parameters of the characterized fault model were set so that the surface trace of the fault model was consistent with distribution of the surface ruptures published by the AIST with reference to Ozawa *et al.* [9] and Yoshida *et al.* [7]. Fig. 3 shows the ground surface projection of the characterized fault model and Fig. 4 shows bird's-eye view of the characterized fault model. Table 1 shows the parameters of the fault model. The characterized fault model consists of six segments: The Hinagu fault (Seg.H); the section connecting the Hinagu fault to the Futagawa fault (Seg.F-H); the southwest part of the Futagawa fault (Seg.F_{SW}); the northeast part of the Futagawa fault (Seg.F_{NE}); and the Idenokuchi fault, which is a normal fault running parallel to the Futagawa fault zone (Seg.I). Two surface ruptures that were confirmed in the central part of Mashiki Town are considered to form the southwest part of Seg.F_{SW} and Seg.F-H. The slip velocity time function of the background region and the SMGAs use the approximate equation of Nakamura and Miyatake [21], which is a Kostrov-type function. The LMGAs use a simple isosceles triangle function. The parameters for determining the shape of the Nakamura-Miyatake slip velocity time function, f_{max} is 4.4 Hz with a reference to Satoh [22]; the rise time t_r is given by $t_r = 0.5 \times W/V_r$, which follows the strong motion prediction recipe [23]. The propagation velocity V_r of the time window of the slip velocity time function was fixed at 2,700 m/s in all segments, and the delay of the start time

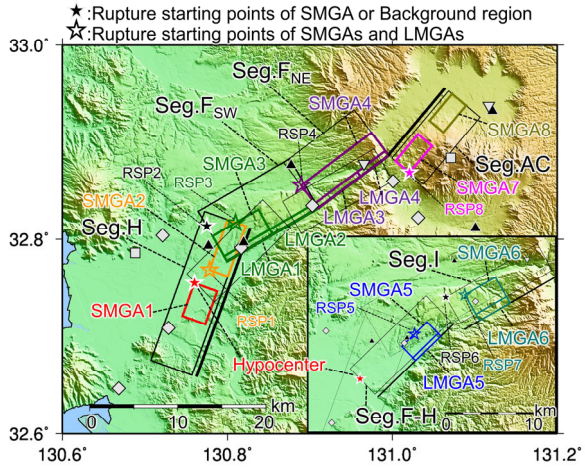

Fig. 3 – Ground surface projection of the characterized fault model. The stars indicate the rupture starting points in each segment. The thick lines show the surface trace of the fault plane.

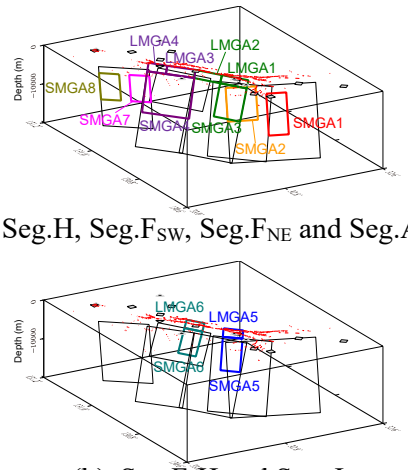

(a) Seg.H, Seg.F_{SW}, Seg.F_{NE} and Seg.AC

(b) Seg.F-H and Seg. I

Fig. 4 – Bird's eye view of the characterzied fault model.

(lag time) was set while comparing the observed records with the theoretical waveforms. The stress drop $\Delta\sigma_a$ of the SMGA and the effective stress σ_b of the background region are parameters related to the maximum

amplitude of the slip velocity time function in the calculations and were determined to be the values shown in Table 1 by confirming consistency with the observed records. SMGA3 and SMGA5 consider the upward rupture propagation effect shown by the previous waveform inversion analysis. It has been pointed out that directivity pulses due to the upward rupture propagation effect also occur in direction parallel to the fault. For the LMGA, the rupture was set to propagate from the rupture starting points in the SMGA that were directly underneath. We compared the spatial distribution of the theoretical ground motions due to the differences in the top depth of the SMGA with the areas of local building damage concentrations in the central part of Mashiki Town and concluded that the upper depth of the SMGAs are defined to be 2 km from the surface in the dip angle direction; the LMGAs are defined from the shallower SMGA to the ground surface [14], which is referenced in this study. The rise times for the LMGAs were determined so that the observation records in the vicinity could be simulated. The rise time at LMGA3 was 2 sec and the rise times at the other LMGAs were set 3 sec. These rise time values are nearly consistent with those used in previous Kumamoto simulations [13, 24, 25]. The rupture starting points of each segment were set so that the time window of the slip velocity time function propagated concentrically from the RSP shown in Table 1 and the relative delay times from the earthquake occurrence time from the JMA were set as shown in Table 2.

Regarding the placement of the source points on the fault plane when calculating the Green's function, for the SMGA and background region, integration points based on the sixth-order Gauss-Legendre formula were placed within a 2 km × 2 km fault element and considered the rupture propagation effects in the fault element. For the LMGA, the distance between the source points and receive point is small, so it is necessary to sufficiently consider the convergence of the calculation accuracies. In this study, for the LMGA, the 2 km × 2 km fault elements were equally divided into 10 × 10 cells and the resulting small faults sizes were 200 m × 200 m. The distance between the 93051 site, nearest to the seismic fault model, is approximately 500 m. The

Table 1 – Parameters of the characterized fault model

Segment		Length (m)	Width (m)	Strike/Dip/Rake (deg.)	Slip (m)	M_0** (Nm)	$\Delta\sigma_a$, σ_b (MPa)	RSP	Lagtime (s)
Seg. H	Background	12,000*	18,000*	200/74/190	0.4	2.95×10^{18}	2.3	Hyp.	1.50
	SMGA1	4,000	10,000		1.3	1.61×10^{18}	11.0	Hyp.	1.50
	SMGA2	6,000	8,000		1.3	1.88×10^{18}	11.0	RSP1	2.00
Seg. F_{SW}	Background	12,000*	18,000*	240/71/200	0.7	3.68×10^{18}	2.3	RSP2	2.80
	LMGA1	6,000	2,000		1.5	3.73×10^{17}	-	RSP3	1.00
	LMGA2	6,000	2,000		1.5	3.73×10^{17}	-	RSP3	1.50
	SMGA3	6,000	8,000		1.5	2.16×10^{18}	11.0 10.0	RSP3	1.60
Seg. F_{NE}	Background	10,000*	18,000*	233/71/200	0.7	1.78×10^{18}	2.3	RSP2	2.80
	LMGA3	6,000	2,000		2.5	6.22×10^{17}	-	RSP4	0.00
	LMGA4	4,000	2,000		2.0	3.31×10^{17}	-	RSP4	0.30
	SMGA4	10,000	10,000		2.5	7.60×10^{18}	11.0	RSP4	0.70
Seg. F-H	Background	12,000	18,000*	226/79/190	0.7	4.02×10^{18}	3.1	Hyp.	1.80
	LMGA5	4,000	2,000	226/79/200	1.5	2.56×10^{17}	-	RSP5	0.00
	SMGA5	4,000	8,000	226/79/190	1.5	1.45×10^{18}	15.0 10.0	RSP5	0.60
Seg. I	Background	12,000	8,000*	240/65/240	0.7	1.27×10^{18}	3.1	RSP6	0.00
	LMGA6	6,000	2,000		2.0	4.97×10^{17}	-	RSP7	0.00
	SMGA6	6,000	6,000		3.0	3.17×10^{18}	15	RSP7	0.00
					2.0	2.11×10^{18}			
Seg. AC	Background	10,000*	18,000*	40/75/220	0.7	2.53×10^{18}	3.1	RSP8	1.00
	SMGA7	4,000	8,000		4.0	3.94×10^{18}	15.0	RSP8	0.00
	SMGA8	4,000	8,000		4.0	3.94×10^{18}	15.0	RSP8	2.50
					3.0	2.96×10^{18}			

* : The length and width including SMGAs (Does not include LMGAs).
** : Seismic moments was calculated using the soil structures of the KMH16 EW direction. The red characters indicate those parameters of Model-03 that were tuned by the FDM.

Table 2 – Rupture delay times at the rupture starting points (RSPs)

RSP	Hypocenter	RSP1	RSP2	RSP3	RSP4	RSP5	RSP6	RSP7	RSP8
Delay time (s)	0.00	2.00	2.00	3.60	6.60	3.30	6.70	8.00	12.30

above is considered to be a sufficient division because the small fault size is less than half of the observation site's fault plane distance [26].

3.2 Simulation of the strong motion records

Fig. 5 shows comparisons of the synthetic results of the time history velocity waveforms and pseudo-velocity response spectra ($_pS_V$) (with a damping constant of 5 % based on the characterized fault model) and the

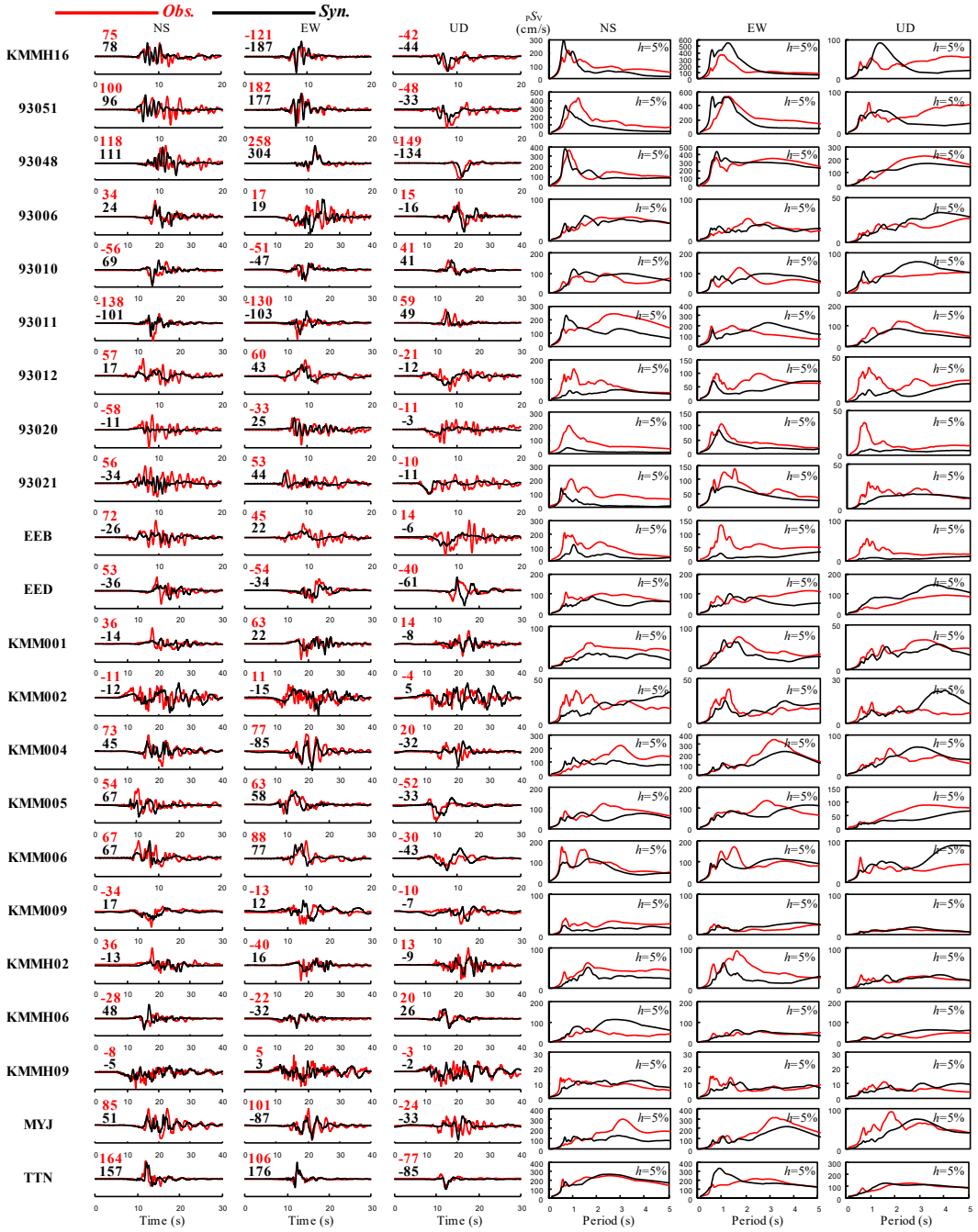

(a) Time history velocity waveforms (b) $_pS_V$ (h=5%)

Fig. 5 – Comparisosn between the observation records (red lines) and the synthetic results (black lines)

Effective period is 0.5 sec or more. The figure on the left shows a comparison of the velocity waveforms and the values in the figure show the PGVs. The red characters are the PGVs of the observation records and the black characters are the PGVs of the synthetic waveforms. The figure on the right shows comparisons between the pseudo-velocity response spectra with a damping constant of 5%.

observation records. The theoretical ground motions calculated from the characterized fault model are in good agreement with the large-amplitude pulse-like motions of approximately 1 sec at KMMH16 and at 93051, located in Mashiki Town. The long-period velocity pulses with periods of approximately 3 sec in the EW and UD components of 93048 are well simulated. The long-period ground motions of the EW components at KMM004 and MYJ, which experienced long-period ground motions with velocity response values of 400 cm/s for approximately 3 sec in Aso City, are also well reproduced. However, since this is a theoretical ground motion calculation assuming a horizontal layered soil structure at the target observation sites, the irregularly layered structure in the Aso Caldera area is not considered. In general, the characterized fault model can effectively reproduce both types of strong motions, such as the large-amplitude velocity pulses near the seismic faults and the small-amplitude ground motions far from the seismic faults. However, for sites 93012 (Kumamoto Chuoku Ooe) and EEB (Kumamoto Nishiku Kasuga) in Kumamoto City, the maximum amplitude was underestimated and the phase was shifted. These differences will be studied in the future using a detailed subsurface structural model.

Fig. 6 shows comparisons between the areal distributions of permanent displacements based on the characterized fault model and the distribution of crustal deformations based on InSAR [27]. The general trends correspond to the actual phenomena and the subsidence trend in the Aso Calera, as indicated by the open circles in Fig. 6, is also reproduced.

4. Evaluation of long-period ground motions in Aso Caldera

4.1 Ground motion calculations using the 3D finite difference method in Aso Caldera

Since the TLM assumes that there are horizontal layered soil structures at the target observation sites, the 3D subsurface irregularities in the Aso Caldera area cannot be addressed. Here, a strong-motion simulation considering the irregularity of the 3D subsurface structure was performed by Nagano [29] using the J-SHIS

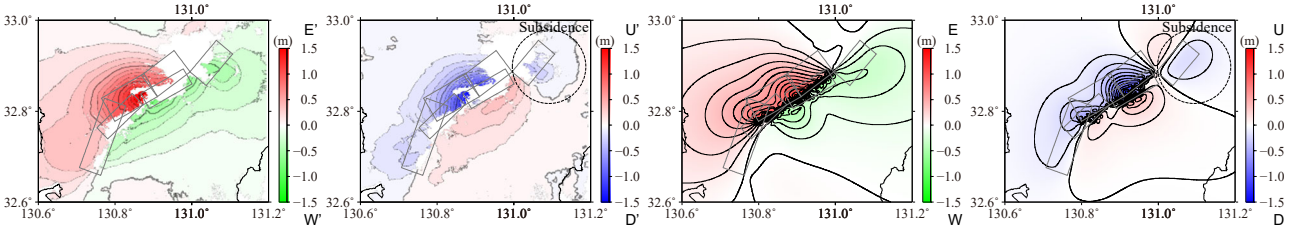

(a) Crustal deformation (Analysis by GSI from ALOS-2 raw data of JAXA)

(b) Peramanent displacement distribtuion based on characterized fault model

Fig. 6 – Comparison between permanent displacement distributions based on characterized fault model and crutal deformation obtained from InSAR data (Geospatial Information Authority of Japan[28])

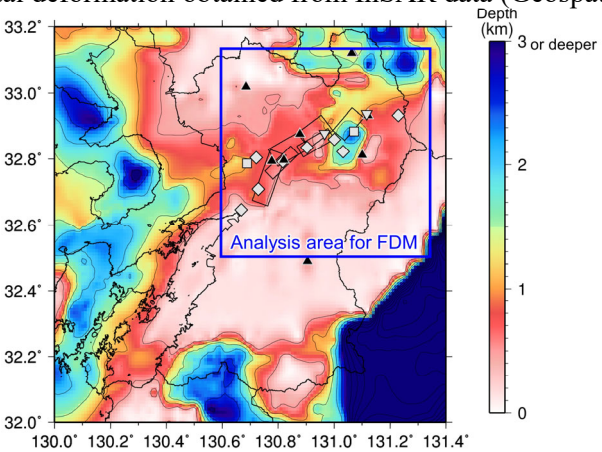

Fig. 7 – Contour map of depths of the seismic bedrock depth model from the J-SHIS V2 model and analysis area of the FDM.

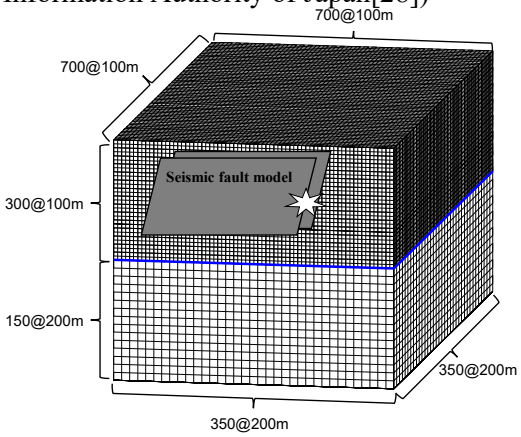

Fig. 8 – Image of grid modeling using the FDM. The seismic fault model is located in the upper region

V2 model and the finite difference method (FDM). Fig. 7 shows the analysis area and a contour map of the depths of the J-SHIS upper surface of the seismic bedrock (VS=3,100 m/s) from the J-SHIS V2 model. The analysis area is 70 km from north to south, 70 km from east to west, and is 60 km deep (upper region 30 km and lower region 30 km). The grid spacing of the analysis was defined as shown in Fig. 8. The damping region was set to 40 grids on the side of the upper region and was set to 20 grids on the side and bottom of the lower region. Since the minimum S-wave velocity in Kumamoto Prefecture in the J-SHIS V2 model was 600 m/s, a band pass filter (0.01 to 1.00 Hz) was applied to the synthesized waveforms. The time interval was 0.005 sec in the upper region, this interval was 0.01 sec in the lower region, and the duration was 81.92 sec.

The following three seismic fault models were considered: the characterized fault model shown in the previous section (Model-01), Model-01 without Seg.AC (Model-02), and the model in which the inner fault parameters of Model-01 were modified to match the observation records in the FDM analysis (Model-03). The parameters of Model-03 after the changes are shown as red characters in Table 1.

Focusing on the ground motion in the Aso Caldera, the velocity waveforms and ${}_{P}S_{V}$ values for each model at the following observation sites are compared in Fig. 9. The observation sites are KMM004; MYJ, located in Aso Caldera; 93006 (Aso City Namino), located on the northeastern part of the outer rim of a Mt. Aso; and KMMH06 (KiK-net Hakusui), located very close to the southern end of Aso Caldera. Focusing on KMM004 and MYJ, Model-01 provides larger amplitudes for the observed ground motions than those from the horizontal layered analysis. The seismic fault model was tuned with inner fault parameters that were targeted for horizontal layered analysis, leading to amplitude overestimations caused by the 3D irregularities in the subsurface structure. The synthetic waveforms from Model-02 without Seg.AC do not reproduce those ground

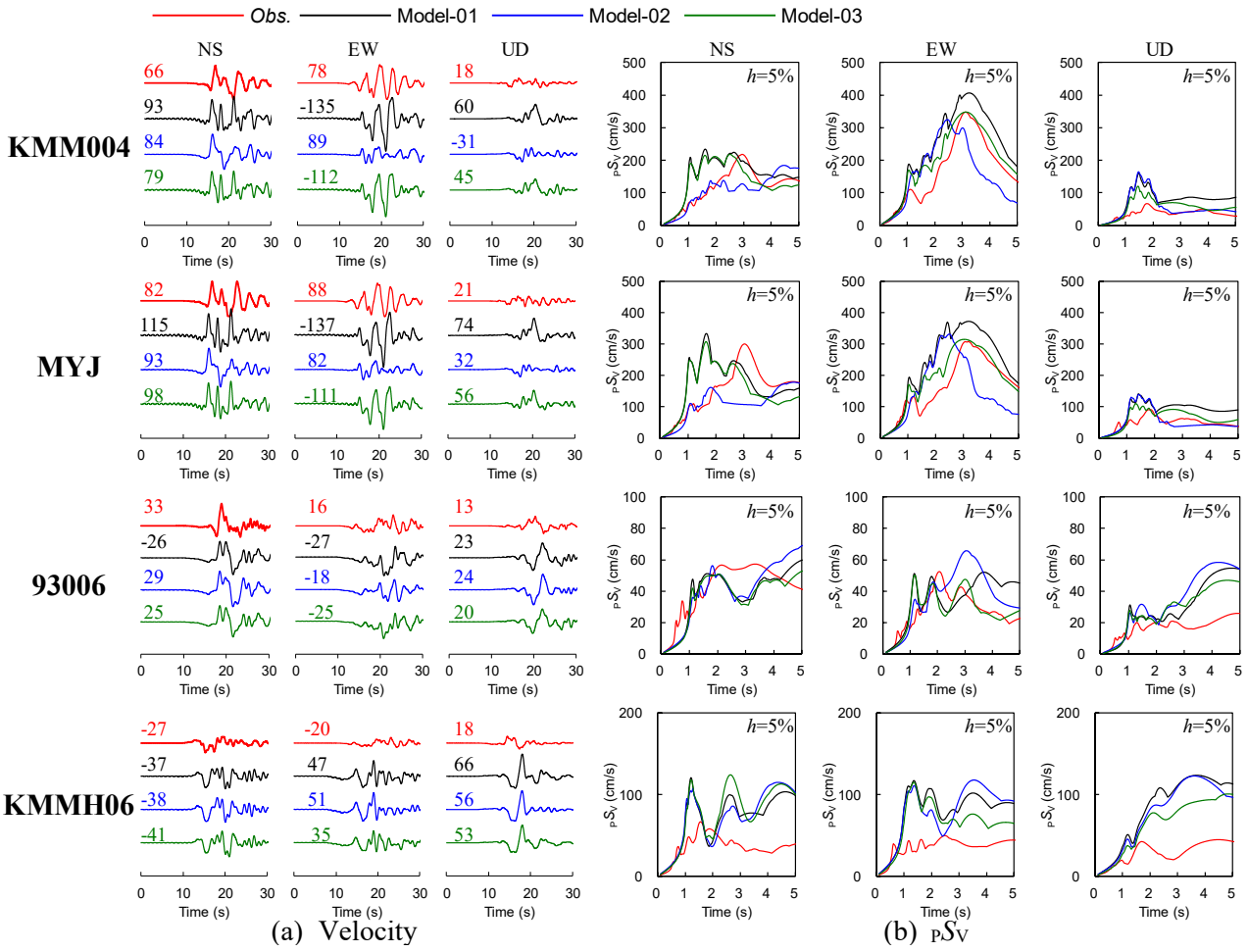

Fig. 9 – Comparisons of velocity waveforms and PSV spectra from the observation records and the synthetic results for four stations near Aso Caldera. The values shown in the velocity waveforms are PGVs

motions with a 3 sec period that are within the main motion portion of the EW component. In Model-03, for which the inner parameters of the fault model were redetermined for FDM analysis, the maximum velocity response level of the EW component with a period of 3 sec shows consistency with the observed records. This indicates that the Aso Caldera segment needs to be considered to reproduce the long-period ground motions with a 3 sec period at KMM004 and MYJ, which cannot be explained by only the 3D modeling. From the comparison of the synthetic results at sites 93006 and KMMH06 from Model-01 and Model-03, there are no significant differences observed, however there are cases where the ${}_{P}SV$ values in the long-period range become larger for the case without Seg. AC. These cases indicate that the sensitivity of the observation sites around Seg.AC is low and that the number of observation sites that can be used to estimate the parameters of Seg.AC is limited. These qualitative trends are the same as presented in the inversion analysis by Yoshida *et al.* [7] and in the analysis by the TLM covered in the previous section. From the above discussion, Seg. AC is indispensable for generating the long-period ground motion with a 3 sec velocity pulse at sites KMM004 and MYJ.

4.2 Generation factors of long-period ground motions in Aso City.

The characterized fault models effectively reproduced the long-period ground motions at sites KMM004 and MYJ in Aso City, whether the method used was a horizontal layered analysis using TLM or was a 3D subsurface structural analyses using the FDM. The contributions from each segment were extracted using Model-01 and the TLM. Fig. 10 shows the horizontal-component observation records at site KMM004, synthetic waveforms by TLM, and contributions from the major segments. The contribution to the synthetic waveforms from site SMGA4 is relatively large for the NS component and this is due to the directivity effect. The contributions from sites SMGA7 and SMGA8 can be ignored for the EW component partly because the observation site is relatively close to Seg. AC.
Fig. 11 shows the transfer function from the seismic bedrock to the ground surface while considering the equivalent nonlinearity for the tuned soil structure. It can be seen that the peak near 0.3 Hz (with a period of approximately 3.3 sec) also contributes to the large amplitudes of the long-period ground motions.

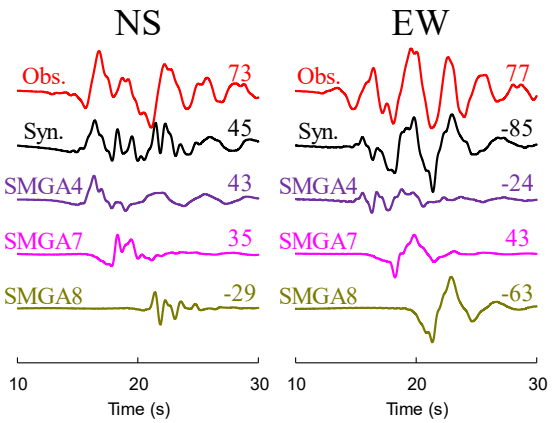

Fig. 10 – Observation records, synthetic waveforms, and the contributions of various segments to the velocity at the KMM004 site.

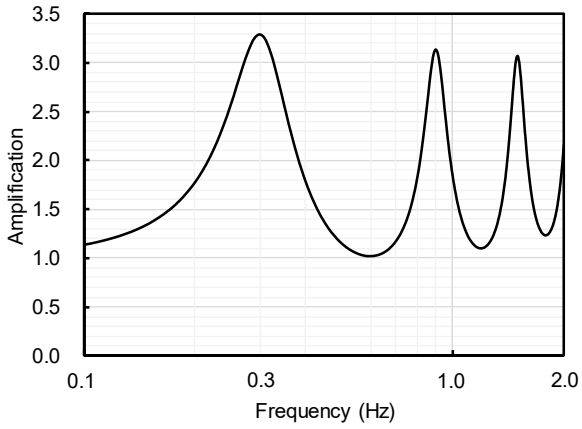

Fig. 11 – The transfer function from the seismic bedrock to the ground surface at the KMM004 site.

4.3 Ground motion evaluations at the seismically isolated hospital building in Aso City

A seismogram for the seismically isolated layer was obtained at a seismically isolated hospital that is located approximately 3.5 km northwest of site KMM004 [3]; digital seismic data were not recorded. The seismogram shows a maximum amplitude of approximately 46 cm, which is the largest displacement observed in a seismically isolated building in Japan. However, if the observed ground motion at site KMM004 is applied to this building, the deformation of the isolated building becomes larger than that indicated by the seismogram. [3]. Fig. 12 shows the orbital plots of the relative displacement responses from the linear response analysis of

the SDOF with an equivalent natural period of 3.2 sec [30] and with damping constant of 15% by the Nigam-Jennings method and using the observed ground motion at site KMM004 and also the seismogram recorded at the seismically isolated hospital building in Aso City. Since the displacement response orbital plot deviates greatly from the seismogram, it is estimated that the ground motion applied at the seismically isolated hospital during the main event was significantly different from the observed record at site KMM004. It has been pointed out that this difference may have been influenced by the differences of the deep soil structure at the two sites. Shigefuji *et al* [31] estimated the 1D S-wave structure under the seismically isolated hospital but the transfer function shows high amplification at approximately 0.3 Hz. In this study, we conducted a parameter analysis by varying the S-wave velocity in the deep part of subsurface structure. Fig. 13 shows the S-wave structure from Shigefuji *et al.* [31] and the adjusted S-wave structure when considering soil nonlinearity. In Case1, a reduction rate of 0.75 was applied to the S-wave velocities where the tuned V_S values were less than 860 m/s. In Case2, a reduction rate of 0.75 was applied to the S-wave velocities where the tuned V_S values were less than 1,020 m/s. Fig. 14 shows the velocity waveform and the displacement response spectrum (S_D) with a damping constant of 15% at the seismically isolated hospital site. It can be seen that the displacement response was reduced for both the NS and EW components by applying a reduction rate of 0.75 to the S-wave velocities. Fig. 15 shows a comparison of the orbital plots of the displacements and the seismogram by linear response

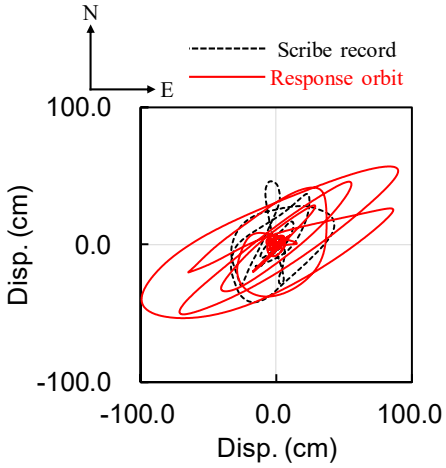

Fig. 12 – Comparison between the hysteresis curve (black line) of the lead-rubber bearings and response displacement orbit by linear analysis.

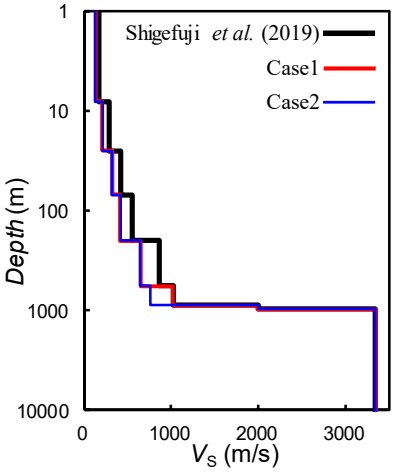

Fig. 13 – Soil profile used for case study and velocity profile of Shigefuji *et al.* (2019)

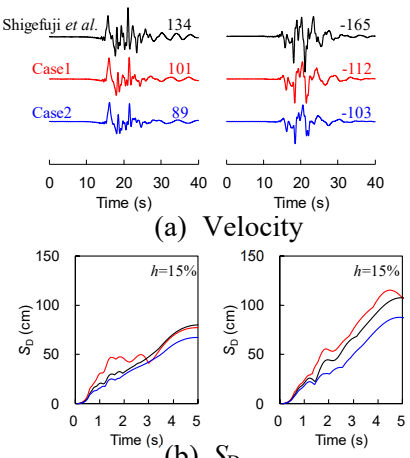

Fig. 14 – Comparison of the synthetic results at a seismically isolated hospital building in Aso City.

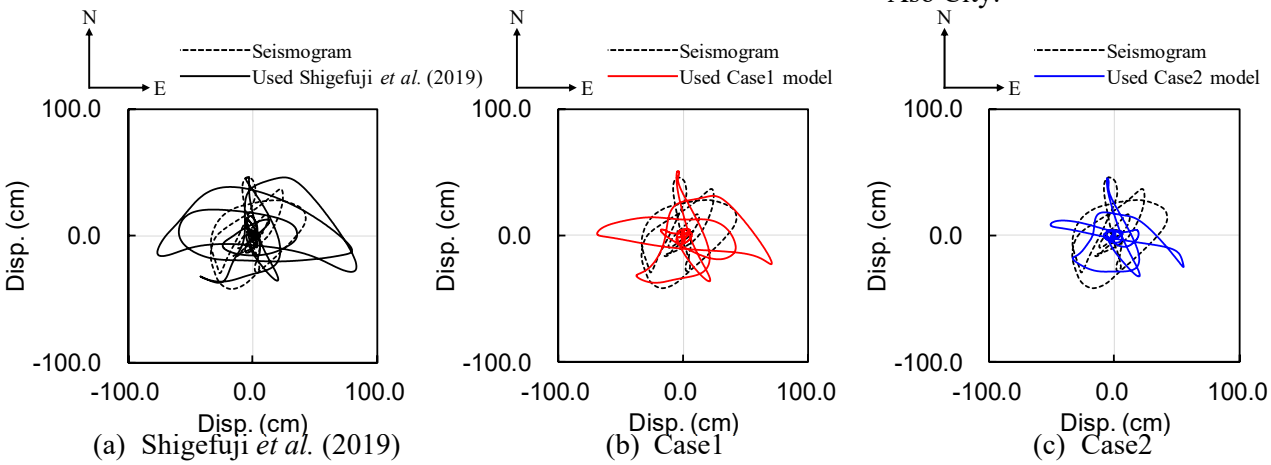

Fig. 15 – Comparison between the hysteresis curve and orbital plots of the response displacements using seismic waves from (a) Shigefuji *et al.* (2019), (b) Case1, and (c) Case2.

analysis with a period of 3.2 sec and a damping constant of 15%, similar to that shown Fig. 12. The response results using the ground motions calculated for the soil structure by Shigefuji *et al.* and in Case1 produce larger orbital plots of the displacements than the seismogram indicates. On the other hand, the orbital plots of the displacement of the response results when using the ground motions calculated from Case2 are at approximately the same level as the seismogram. From these results, it is possible to explain the differences in ground motion between site KMM004 and the seismically isolated hospital in Aso City as being due to the differences in the site amplification characteristics during the main seismic event when considering the soil nonlinearity in the deep part of the subsurface structure with large V_S values.

5. Conclusions

In this study, we constructed a characterized fault model for simulating the strong-motion records around the seismic fault during the 2016 Kumamoto earthquake by using the fault models in a previous study. The characterized fault model reproduced the large-amplitude pulses in Mashiki Town and Nishihara Village, which are adjacent to the surface ruptures and to the long-period ground motions in Aso City. The long-period ground motions in Aso City can be simulated by two SMGAs in the segment that is in Aso Caldera area. The amplification effect from the 3D subsurface structure is small. The differences between the ground motions at site KMM004 and at the seismically isolated hospital site in Aso City can be explained by the differences in site amplification during the main seismic event by considering the soil nonlinearity in the deep part of the subsurface structure with high S-wave velocities.

6. Acknowledgements

In this study, we used the strong motion data of KiK-net and K-NET from National Research Institute for Earth Science and Disaster Resilience, Japan Meteorological Agency, Kumamoto prefectural government, and Kyushu Railway Company. Some figures were created using the GMT and Geographical Information Authority of Japan map image data and Geographical Information Authority of Japan 50 m mesh elevation data. The ownership of the original data of ALOS-3 raw data belongs to JAXA. I would like to thank Dr. Xin Wang, assistant professor of Tokyo University of Science, for her great cooperation in preparing this paper.

7. References

[1] Shirahama, Y. et al.: Characteristics of the surface ruptures associated with the 2016 Kumamoto earthquake sequence, central Kyushu, Japan, Earth, Planets and Space, Vol. 68:191, DOI:10.1186/s40623-016-0559-1, 2016.10

[2] Building Research Institute: Quick Report on Field Surveys and Subsequent Investigations of Building Damage Following the 2016 Kumamoto Earthquake,2016.9 (in Japanese)

[3] Takayama, M. and Morita, K.: A study on the response of seismically isolated hospital in Aso during 2016 Kumamoto earthquake, Summaries of Technical Papers of Annual Meeting, Architectural Institute of Japan, Structures-II, pp. 1051-1052, 2017.8 (in Japanese)

[4] Asano, K. and Iwata, T.: Source rupture processes of the foreshock and mainshock in the 2016 Kumamoto earthquake sequence estimated from the kinematic waveform inversion of strong motion data, Earth, Planets and Space, Vol. 68:147, DOI: 10.1186/s40625-016-0519-9, 2016.8

[5] Hikima, K.: Source rupture processes of the 2016 Kumamoto earthquake and its foreshock inferred from strong motion waveform, JAEE annual meeting 2016, P4-11, 2016.9 (in Japanese)

[6] Kubo, H., Suzuki, W., Aoi, S. and Sekiguchi, H.: Source rupture processes of the 2016 Kumamoto, Japan, earthquakes estimated from strong-motion waveforms, Earth, Planets and Space, Vol. 68: 161, DOI: 10.1186/s40623-016-0536-8, 2016.10

[7] Yoshida, K. et al.: Source process of the 2016 Kumamoto earthquake (Mj7.3) inferred from kinematic inversion of strong-motion records, Earth, Planets and Space, Vol. 69:64, DOI: 10.1186/s40623-017-0649-8, 2017.5

[8] Kobayashi, H., Koketsu, K. and Miyake, H.: Rupture processes of the 2016 Kumamoto earthquake sequence: Causes for extreme ground motions, Geophysical Research Letters, Vol. 44: 6002-6010, DOI: 10.1002/2017GL073857, 2017.6

[9] Ozawa, T., Fujita, E. and Ueda, H.: Crustal deformation associated with the 2016 Kumamoto earthquake and its effect on the magma system of Aso volcano, Earth, Planets and Space, Vol. 68: 186, DOI: 10.1186/s40623-016-0563-5, 2016.11

[10] Toda, S., Kaneda, H., Okada, S., Ishimura, D. and Mildon, Z.: Slip-partitioned surface ruptures for the Mw 7.0 16 April 2016 Kumamoto, Japan, earthquake, Earth, Planets and Space (2016), Vol. 68: 118, doi: 10.1186/s40623-016-0560-8, 2016

[11] Tanaka, S., Kaneda, J., Hikima, K. and Hisada, Y.: Characterized fault model for prediction of long-period ground motions containing permanent displacement in the near-fault region, Journal of Structural and Construction Engineering (Transactions of AIJ), Vol. 83, No. 752, pp. 1525-1535, 2018.10 (in Japanese with English abstract)

[12] Hikima, K., Tanaka, S.: Reanalysis for the source process of the 2016 Kumamoto mainshock using strong motions, Presentation paper of Seismological Society of Japan Fall Meeting of 2018, S14-P18, 2018.10 (in Japanese)

[13] Matsumoto, Y., Miyakoshi, K. and Takahama, T.: Characterized source model for evaluating long-period (more than 2s-) ground motion including permanent displacement of the 2016 Kumamoto earthquake (Mj7.3), The 15th Japan Earthquake Engineering Symposium, PS1-01-17, pp. 2786-2795, 2018.12 (in Japanese with English abstract)

[14] Kido, T., Nagano, M. and Hikima, K.: Simulation and spatial distribution of strong ground motions adjacent to seismic faults during the 2016 Kumamoto earthquake, Journal of Structural and Construction Engineering (Transactions of AIJ), Vol. 84, No. 757, pp. 373-383, 2019.3 (in Japanese with English abstract)

[15] Nagano, M. and Watanabe, T.: Improvement of calculation precision of theoretical ground motions using thin layer method and its verification, AIJ Journal of Technology and Design, Vol. 13, No. 26, pp. 451-456, 2007.12 (in Japanese with English abstract)

[16] Nagano, M. and Koyama, T.: Improvement of calculation precision of theoretical ground motions using thin layer method and its verification, Part 2, AIJ Journal of Technology and Design, Vol. 17, No. 35, pp. 55-59, 2011.2 (in Japanese with English abstract)

[17] Hisada, Y., Nagano, M., Nozu, A. and Miyakoshi, K.: Benchmark tests for strong ground motion prediction methods: Case for theoretical methods (Part 1), AIJ journal of Technology and Design, Vol. 17, No. 35, pp. 43-48, 2011.2 (in Japanese with English abstract)

[18] Awata, Y., Shirahama, Y. and Kumahara, Y.: Integration of surface deformation information associated with the 2016 Kumamoto earthquake, Comprehensive active fault survey based on the 2016 Kumamoto earthquake, 2016-2018 report, Research and Development Bureau, Ministry of Education, Culture, Sports, Science and Technology, Kyushu University. (in Japanese)

[19] National Institute of Advanced Industrial Science and Technology (2019) Active Fault Database April 26, 2019 Edition,National Institute of Advanced Industrial Science and Technology Research Information Database DB095 , AIST, https://gbank.gsj.jp/activefault/

[20] Fujiwara, H. *et al.*: Some improvements of seismic hazard assessment based on the 2011 Tohoku earthquake, Technical Note of the National Research Institute for Eart Science and Disaster Prevention, No. 379, 2012.12 (in Japanese)

[21] Nakamura, H. and Miyatake, T.: An approximate expression of slip velocity time functions for simulation of near-field strong ground motions, Zisin, Vol. 53, pp. 1-9, 2000.7 (in Japanese with English abstract)

[22] Satoh, T.: Broadband source characteristics of the 2016 Kumamoto earthquake estimated from strong motion records, Journal of Structural and Construction Engineering (Transactions of AIJ), Vol. 82, No. 741, pp. 1707-1717, 2017.11 (in Japanese with English abstract)

[23] The Headquarters for Earthquake Research Promotion: Strong ground motion prediction method for earthquake with specified source faults (“Recipe”), April, 2017, https://www.jishin.go.jp/main/chousa/17_yosokuchizu/recipe.pdf, (accessed 2020-01-07) (in Japanese)

[24] Irikura, K., Kurahashi, S. and Matsumoto, Y.: Extension of characterized source model for long-period ground motions in near-fault area, Pure Appl. Geophys. (2019), https://doi.org/10.1007/s00024-019-02283-4, 2019.8

[25] Oana, A., Dan, K., Miyakoshi, J., Fujiwara, H. and Morikawa, N.: Study on the method of strong motion prediction at very close to the fault trace for the 2016 Kumamoto earthquake, Journal of Japan Association for Earthquake Engineering, Vol. 19, No. 6, 2019.10 (in Japanese with English abstract)

[26] Kido, T., Nagano, M. and Hikima, K.: Verification of theoretical evaluation for near fault seismic ground motion by thin layer method, The 15th Japan Earthquake Engineering Symposium, OS2-04-08, pp. 1434-1443, 2018.12 (in Japanese with English abstract)

[27] Ueshiba, H., Miura, Y., Miyahara, B., Nakai, H., Honda, M., Kakitage, Y. and Yamashita, T.: Crustal deformation of the 2016 Kumamoto Earthquake detected by ALOS-2 InSAR images, Journal of the Geospatial Information Authority of Japan, No. 128, 2016

[28] Geospatial Information Authority of Japan: Information about 2016 Kumamoto earthquake, SAR analysis results, (ALOS-2), http://maps.gsi.go.jp/#11/32.926284/130.735931/&base=std&ls=std%7Curgent_earthquake_20160414kumamoto_p023dr_p135ar_qe_25d%2C0.7%7C20160414kumamoto_epicenter%7Curgent_earthquake_qegrd_cont10cm_cut10%2C0.7&blend=0&disp=1111&lcd=urgent_earthquake_20160414kumamoto_p023dr_p135ar_qe&vs=c1j0h0k0l0u0t0z0r0s0m0f1&d=vl (accessed 2019-12-01)

[29] Nagano, M.: Evaluation of Strong Ground Motions in Kobe Area During the 2000 Tottori-ken Seibu Earthquake using 3D Finite Difference Method with Variable Grid Spacing and Time increment, J. Struct. Constr. Eng., AIJ, No. 580, pp. 43-50, 2004.6 (in Japanese with English abstract)

[30] Yamamoto, H. *et al.*: Seismic isolated hospital that continued functioning in the 2016 Kumamoto earthquake, Proceedings of the 12th Japan-China Joint Conference on Structural Engineering, 2017.9 (in Japanese with English abstract)

[31] Shigefuji, M. *et al.*: Estimation of S-wave velocity structures in the north-eastern Aso caldera using microtremor array observations, Summaries of Technical Papers of Annual Meeting, Architectural Institute of Japan, Structures-II, pp. 1051-1052, 2019.9 (in Japanese)

